and in this region, τ oscillates with distance about the value measured at large separation [this effect can be described either as classical modifications or cavity quantum electrodynamic effects in a "bad cavity" as defined in (*28*)].

Some of the maximum values near the middle are well above the far-field bulk $\langle\tau\rangle$ (compare ranges in Fig. 3 to the dashed line). Two factors may contribute to values larger than the bulk lifetime: (i) There could be an inhomogeneous distribution of unperturbed τ values, or (ii) spontaneous emission suppression may affect τ near the center of the probe. An independent means of measuring unperturbed single molecule lifetimes is needed to establish the level of perturbation in the center of the probe. Near the metal edges of the aperture, τ is decreased by at least a factor of 3; fluorescence certainly is quenched near the metal edges.

Our results highlight an important aspect of single molecule experiments; namely, a single molecule can be used as a point probe that displays dramatic fluorescence lifetime variations near an NSOM probe, whereas ensemble measurements only provide spatially averaged information. Because the lifetime variations are repeatable, NSOM provides a means of altering the environment of a single molecule and its decay kinetics. Single molecule NSOM experiments will provide important tests for near-field theories that incorporate the physical effects of radiators near metallic structures. In addition, single molecules will be useful as calibration probes for individual NSOM tips.

Note added in proof: Single molecule detection by conventional optical microscopy was recently reported (*29*). This method could be used as an independent technique to explore unperturbed inhomogeneous lifetime distributions.

REFERENCES AND NOTES

1. E. B. Shera, N. K. Seitzinger, L. M. Davis, R. A. Keller, S. A. Soper, *Chem. Phys. Lett.* **174**, 553 (1990).
2. C. W. Wilkerson, P. M. Goodwin, W. P. Ambrose, J. C. Martin, R. A. Keller, *Appl. Phys. Lett.* **62**, 2030 (1993).
3. P. M. Goodwin, C. W. Wilkerson, W. P. Ambrose, R. A. Keller, *Proc. SPIE* **1895**, 79 (1993).
4. M. D. Barnes, K. C. Ng, W. B. Whitten, J. M. Ramsey, *Anal. Chem.* **65**, 2360 (1993).
5. R. Rigler, J. Widengren, Ü. Mets, in *Fluorescence Spectroscopy: New Methods and Applications*, O. S. Wolfbeis, Ed. (Springer-Verlag, Berlin, 1993), p. 13.
6. S. A. Soper, Q. L. Mattingly, P. Vegnuta, *Anal. Chem.* **65**, 740 (1993).
7. W. E. Moerner and L. Kador, *Phys. Rev. Lett.* **62**, 2535 (1989).
8. M. Orrit and J. Bernard, *ibid.* **65**, 2716 (1990).
9. W. P. Ambrose and W. E. Moerner, *Nature* **349**, 225 (1991).
10. W. E. Moerner and T. Basché, *Angew. Chem. Int. Ed. Engl.* **32**, 457 (1993).
11. M. Pirotta *et al.*, *Chem. Phys. Lett.* **208**, 379 (1993).
12. E. Betzig and R. J. Chichester, *Science* **262**, 1422 (1993).
13. W. P. Ambrose, P. M. Goodwin, J. C. Martin, R. A. Keller, *Phys. Rev. Lett.* **72**, 160 (1994).
14. ———, *Proc. SPIE* **2125**, 2 (1994).
15. R. C. Dunn, E. V. Allen, S. A. Joyce, G. A. Anderson, X. S. Xie, *Ultramicroscopy*, in press.
16. J. K. Trautman, J. J. Macklin, L. E. Brus, E. Betzig, *Nature* **369**, 40 (1994).
17. U. Dürig, D. W. Pohl, F. Rohner, *J. Appl. Phys.* **59**, 3318 (1986).
18. K. H. Drexhage, *Prog. Opt.* **12**, 163 (1974).
19. N. K. Seitzinger, K. D. Hughes, F. E. Lytle, *Anal. Chem.* **61**, 2611 (1989).
20. D. C. Nguyen, R. E. Muenchausen, R. A. Keller, N. S. Nogar, *Opt. Commun.* **60**, 111 (1986).
21. M. Lieberherr, C. Fattinger, W. Lukosz, *Surf. Sci.* **189**, 954 (1987).
22. E. Betzig, J. K. Trautman, T. D. Harris, J. S. Weiner, R. L. Kostelak, *Science* **251**, 1468 (1991).
23. E. Betzig and J. K. Trautman, *ibid.* **257**, 189 (1992).
24. L. Q. Li and L. M. Davis, *Rev. Sci. Instrum.* **64**, 1524 (1993).
25. The reason for the multiply lobed images was described in (*12*): An optical dipole is excited by the component of the field along the dipole axis. The field bows out from the aperture and is normal to the aperture edges. A single optical dipole oriented perpendicular to the aperture is excited most strongly by the edge fields, and lobes form as the point-like molecule images one component of the near field.
26. A. L. Huston and C. T. Reimann, *Chem. Phys.* **149**, 401 (1991).
27. J. N. Demas and B. A. DeGraff, *Sensors Actuators B* **11**, 35 (1993).
28. T. W. Mossberg and M. Lewenstein, in *Cavity Quantum Electrodynamics*, P. R. Berman, Ed. (Academic Press, Boston, MA, 1994), p. 173.
29. M. Ishikawa, K. Hirano, T. Hayakawa, S. Hosoi, S. Brenner, *Jpn. J. Appl. Phys.* **33**, 1571 (1994).

9 March 1994; accepted 31 May 1994

Fine Structure of the Landers Fault Zone: Segmentation and the Rupture Process

Yong-Gang Li,* John E. Vidale, Keiiti Aki, Chris J. Marone, William H. K. Lee

Observations and modeling of 3- to 6-hertz seismic shear waves trapped within the fault zone of the 1992 Landers earthquake series allow the fine structure and continuity of the zone to be evaluated. The fault, to a depth of at least 12 kilometers, is marked by a zone 100 to 200 meters wide where shear velocity is reduced by 30 to 50 percent. This zone forms a seismic waveguide that extends along the southern 30 kilometers of the Landers rupture surface and ends at the fault bend about 18 kilometers north of the main shock epicenter. Another fault plane waveguide, disconnected from the first, exists along the northern rupture surface. These observations, in conjunction with surface slip, detailed seismicity patterns, and the progression of rupture along the fault, suggest that several simple rupture planes were involved in the Landers earthquake and that the inferred rupture front hesitated or slowed at the location where the rupture jumped from one to the next plane. Reduction in rupture velocity can tentatively be attributed to fault plane complexity, and variations in moment release can be attributed to variations in available energy.

The major crustal faults that accommodate tectonic motion are complex sets of slip planes, which are probably influenced by the presence of fault gouge and fluid, and exhibit deformation that ranges from steady to stick-slip (*1*). The part of the fault that slips at depth in an earthquake is quite narrow, so it is difficult to delineate the features that make faults segment into distinct earthquakes. Recently, short-wavelength seismic waves that travel mainly within the fault zone have been detected (*2*). Because the fault zone is characterized by slower velocities than the surrounding intact rock, probably as a result of intense brecciation and possibly high fluid pressure, it forms a waveguide. When an earthquake occurs in the fault zone, some seismic energy is trapped in the waveguide and propagates as normal modes that are formed by the constructive interference of the multiple reflections at boundaries between the low-velocity fault zone and the high-velocity surrounding rock. Such waves are similar to surface or channel waves.

In this report, we illustrate fault zone–guided waves from aftershocks of the Landers earthquakes (*3*, *4*). On the basis of the observation and modeling of the guided waves, we document the fine velocity structure in the heart of the fault zone that ruptured in the 28 June 1992 magnitude M7.4 Landers earthquake.

In the months after the main shock, linear seismic arrays crossing the fault trace were installed at nine locations along the rupture plane for the purpose of detecting fault-guided waves (*3*, *4*). The array at recording site 8 had 22 three-component receivers spread over 1000 m across the

Y.-G. Li and K. Aki, Department of Earth Sciences, University of Southern California, Los Angeles, CA 90089, USA.
J. E. Vidale and W. H. K. Lee, U.S. Geological Survey, Menlo Park, CA 94025, USA.
C. J. Marone, Department of Earth, Atmospheric, and Planetary Sciences, Massachusetts Institute of Technology, Cambridge, MA 02139, USA.
*To whom correspondence should be addressed.

main shock fault trace (5). The array at site 3 consisted of six instruments spread across 2 km. During 5 days in October 1992, 250 aftershocks were recorded at the site 8 array; in July 1992, 100 were recorded at site 3 (Fig. 1).

As has been described previously (2, 6), the low-velocity fault zone traps and focuses seismic energy. In the Landers fault zone, the seismic energy in the frequency range 3 to 6 Hz, most of it trapped in the fault zone, traveled slowly. The seismic energy at a frequency lower than 3 Hz, which penetrated a few tens to hundreds of meters into the surrounding rock, traveled more rapidly. Because of this dispersion and concentration of wave-guided energy in and near the fault zone, these waves can be used as a probe of the state of the fault zone (Fig. 2).

We compared synthetic fault zone–guided waves with observed seismograms for two earthquakes: one occurring in the fault zone and one occurring outside it (Fig. 3). The comparison showed that, to generate significant guided waves, earthquakes must be in or near (a few hundred meters offset from) the low-velocity zone, the low-velocity zone must be continuous, and the thickness of basin sediments above the fault zone and

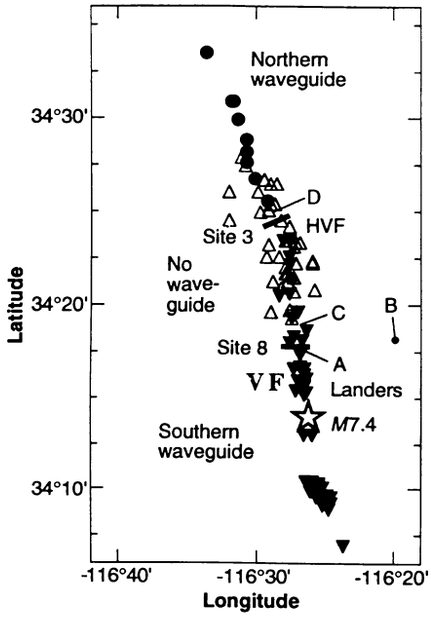

Fig. 1. Map of the study region showing the locations of two recording sites (site 3 and site 8, denoted by solid lines) and aftershocks that were used in this study. All events are relocated (*20*). HVF, Homestead Valley fault; JVF, Johnson Valley fault. Events that showed fault zone–guided waves at site 8 are shown by solid triangles, events that showed guided waves at site 3 are shown by solid circles, and events that did not show guided waves at sites 3 and 8 are shown by open triangles. Events used in Figs. 3 and 5 (Table 1) are labeled by A through D.

Table 1. Locations of events used in Figs. 3, 4, and 5.

Event	Date (October 1992)	Time (GMT)	Latitude (°N)	Longitude (°W)	*M*	Depth (km)
A	16	12:06	34°17.33	116°26.72	0.5	6.7
B	14	01:31	34°17.74	116°21.26	0.9	4.0
C	16	07:17	34°19.34	116°26.72	0.7	10.7
D	15	11:05	34°24.93	116°29.67	1.9	3.7
1	12	09:56	34°16.64	116°26.80	2.2	2.8
2	12	00:42	34°15.50	116°26.41	2.1	3.2
3	13	07:22	34°13.11	116°25.77	1.8	4.3
4	16	06:24	34°12.34	116°25.91	2.0	4.1
5	13	04:02	34°09.19	116°25.14	2.5	3.8
6	16	07:50	34°09.05	116°25.55	2.5	9.7

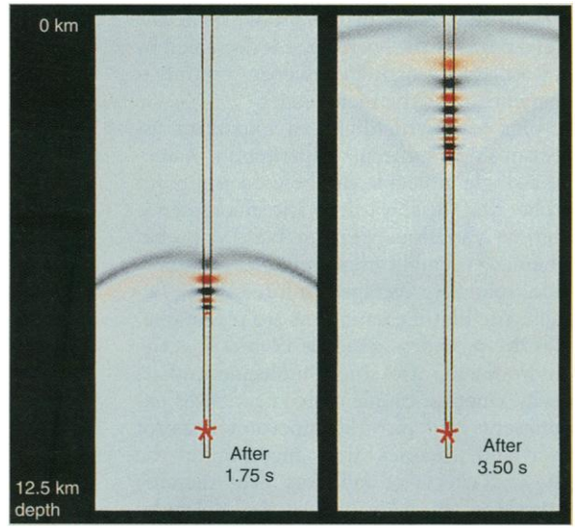

Fig. 2. Cross section of the Landers fault zone and finite-difference simulation of fault-guided waves of an earthquake (red star) at a depth of 9.75 km. Blue and red indicate the opposite polarities of displacement, and white indicates no displacement. The fault-parallel ground displacement 1.75 s after the earthquake is shown at the left, and the displacement 3.5 s after the earthquake is shown at the right. The shear velocity is assumed to be 2.1 km/s in the fault zone and 3.1 km/s outside the zone. The fault zone is 180 m wide at the surface and tapers to 120 m at a depth of 10 km. The simulation is two-dimensional and models the fault-parallel horizontal component of displacement, with a fourth-order in space and second-order in time finite-difference method (*21*).

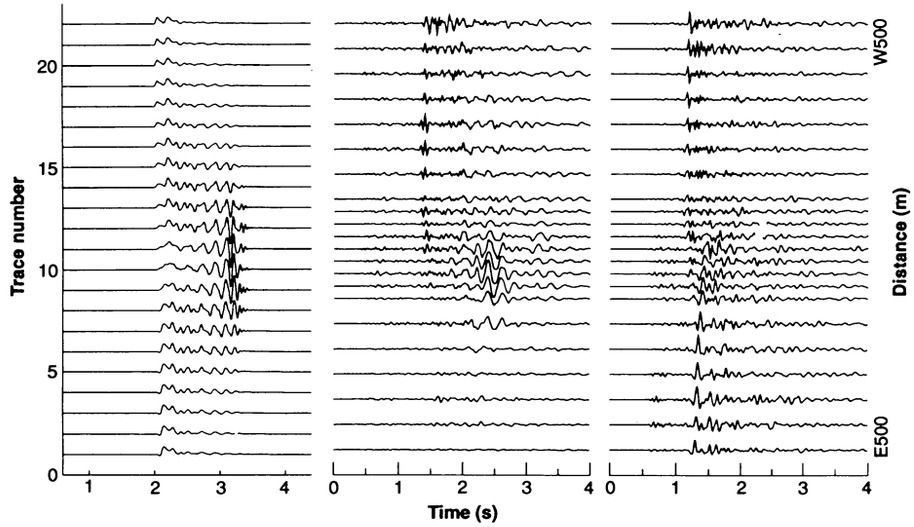

Fig. 3. Fault zone–parallel component seismograms. (**Left**) Synthetic seismograms computed with the model shown in Fig. 2. (**Middle**) Observations from the array at site 8 for aftershock A (Table 1), which occurred on the fault. (**Right**) Seismograms recorded for aftershock B (Table 1), which did not occur on the fault. The aftershocks are located in Fig. 1. The fault zone–guided waves are visible at the stations located near the surface fault trace in the simulations and for the event within the fault zone but not for the event outside the fault zone.

country rock must be less than several times the fault zone thickness.

Seismograms of six events occurring in the fault zone south of the fault bend (Fig. 1 and Table 1) recorded at the seismic array at site 8 on the Johnson Valley fault show that the separation between the *S*-wave arrival and the arrival of a fault zone–guided wave in the frequency range from 2 to 3 Hz increased as the hypocentral distance increased (Fig. 4). The delay of more than 1 s is a result of the wave velocity of the shear energy propagating along the fault zone being slower than in the surrounding country rock (*3*, *4*). The data from these events support a continuous fault plane waveguide along the southern Landers rupture plane.

A discontinuity of the fault plane waveguide at the fault bend is illustrated in the data shown in Fig. 5 for two earthquakes occurring south and north of the fault bend, respectively. The seismic array at site 8 south of the bend did not register guided waves from the event north of the bend, whereas it registered clear longer period guided waves arriving after the *S*-waves at the central stations located nearest the fault trace for the event south of the bend. On the other hand, we observed guided waves at site 3, located north of the fault bend, only when events occurred within the fault zone north of the bend [figures 18 and 20 of (*3*)]. These observations imply that there is a break in the fault zone waveguide at the fault bend.

There is a region around the fault bend from which aftershocks did not produce guided waves (Fig. 1). The pattern of the aftershocks that excited fault zone–guided waves was more linear than the overall aftershock pattern. But events occurring at the fault bend did not excite guided waves. This result suggests that the fault zone waveguide is discontinuous at the fault bend.

The lack of a continuous waveguide at the fault bend requires that either the rupture plane is discontinuous or the low-velocity structure thins or thickens dramatically. Simulations show that a 20° kink in a thin low-velocity layer does not affect the propagation of guided waves. This evidence also suggests that the waveguide is discontinuous at the fault bend.

The fault bend coincided with a slowdown in the propagation of the rupture (*7*, *8*) and a minimum in surface slip (*9*, *10*). The pattern of moment release, on the other hand, is more complicated (*7*, *8*). There are two or three patches of high moment release, but their relation to fault plane geometry is not clear. The rupture velocity from the hypocenter to the fault bend was 3 to 4 km/s (*7*, *8*). The rupture then either hesitated for 5 to 10 s or slowed to 2 km/s (*7*, *8*). The overall velocity was about 2.5 to 2.7 km/s along the entire rupture trace. The minimum in surface slip near the bend probably results from more complicated deformation near the surface than at depth, because there is no clear minimum in moment release at the fault bend. This interpretation of surface slip is supported by data showing that the waveguide is discontinuous at the bend from the surface to a depth of at least 5 to 6 km (Fig. 6).

Other earthquakes have shown a similar hesitation in their rupture (*11*). The 1984 Morgan Hill earthquake (*12*) hesitated 0.5 to 1.0 s before rupturing an asperity (*12*). There is evidence from aftershocks for fault plane complexity where the rupture hesitat-

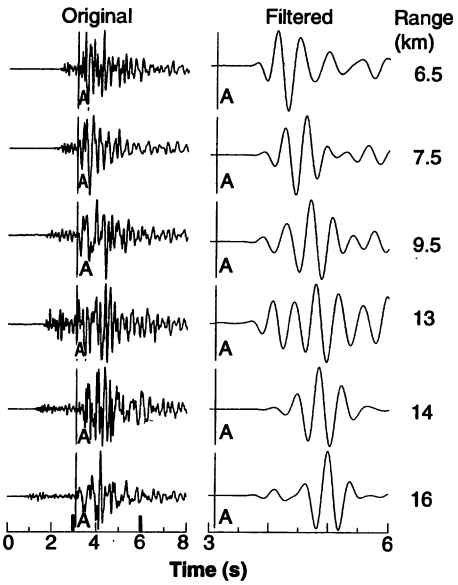

Fig. 4. (**Left**) Fault zone–parallel horizontal component seismograms recorded at a station located near the fault trace at site 8 for six aftershocks (labeled by 1 through 6 in Table 1) that occurred on the fault at various hypocentral distances from the seismic array. Seismograms are plotted with the *S*-wave onset aligned by a vertical line (marked by A). (**Right**) Plot of 2- to 3-Hz bandpass-filtered seismograms shown with an expanded time scale between 3 and 6 s.

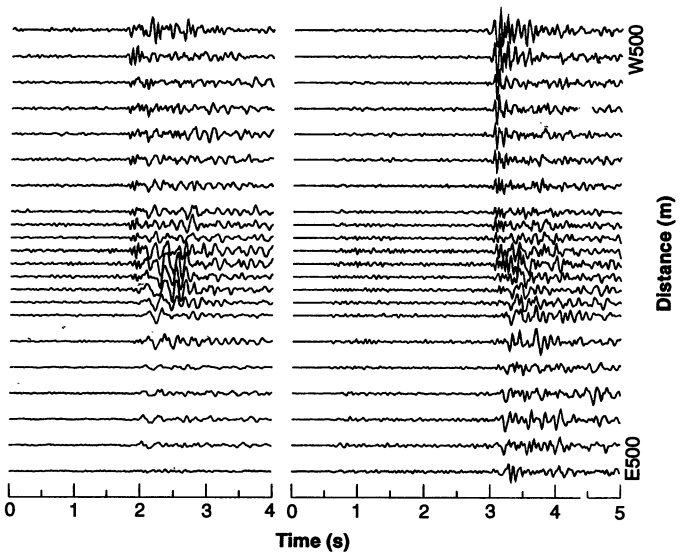

Fig. 5. (**Left**) Fault zone–parallel horizontal component seismograms recorded across the seismic array at site 8 for aftershock C (Table 1), which occurred on the fault south of the fault bend. (**Right**) Fault zone–parallel horizontal component seismograms recorded for aftershock D (Table 1), which occurred on the fault north of the bend. These aftershocks are located in Fig. 1.

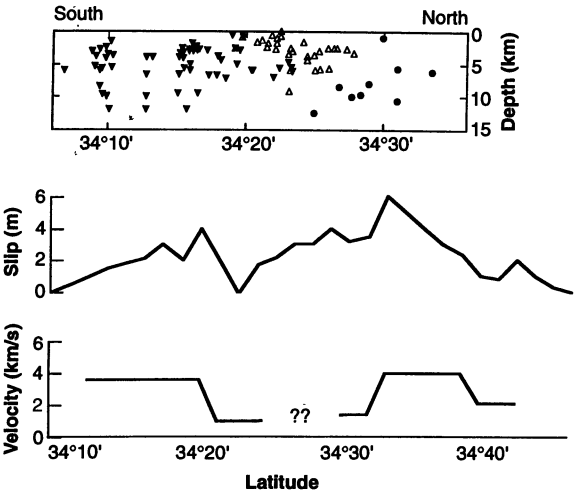

Fig. 6. (**Top**) Cross section of the fault showing the events that showed fault zone–guided waves at site 8 (solid triangles), events that showed guided waves at site 3 (solid circles), and events that did not excite guided waves (open triangles). (**Middle**) Profile of measured surface displacement (*10*). (**Bottom**) Estimate of spatial variation of rupture velocity (*7*).

ed, but it is equivocal (*12*). The 1968 Borrego Mountain earthquake shows a pattern similar to that of the Landers event: The rupture appeared to hesitate at a dilatational stepover, where surface slip was a minimum (*13*), but geodetic surveys show no clear minimum in slip at depth at the stepover (*14*).

Our observations of fault zone–guided waves are consistent with some aspects of existing fault-zone rupture models. The separation of simple crack by a barrier is a feature of the specific barrier model (*15*). For an M7.4 event, this model predicts that cracks have a diameter of 15 km, close to the dimension of the waveguides that we observed. Other models describe alternation between rupture near the Rayleigh velocity and slower rupture propagation (*16*).

We interpret the Landers rupture as a combination of rapid rupture on planar fault surfaces and hesitation at fault surface complexity. The rupture history is a function of fault geometry rather than available strain energy. Hesitancy is an important determinant of rupture energetic and strong motion. The ability to use guided waves to locate the fault plane precisely furthers an understanding of the rupture process (*17*).

It is not clear whether the fault zone waveguide originated primarily during the recent Landers earthquake or whether it represents a wear zone that has accumulated over geological time. In the former view, which has its roots in fracture mechanics, the waveguide may represent the width of the process zone, a zone of inelastic deformation around the propagating crack tip.

Theoretical work or fault mechanics suggests that P/L is of order 10^{-2}, where P is the dynamic process zone width and L is the rupture length (*18*). If we take L = 30 km, the length of the two main subfaults, P is 300 m, which is consistent with our observations of the width of the fault zone waveguide. This value is not conclusive as to the origin of the waveguide, however, because the same scaling arguments yield a total fault displacement, d, of 200 m to 2 km, which is a reasonable value for the recent net offset of the faults. Our data do not indicate that the fault zone has widened with depth. The 200-m width of the waveguide is consistent with the theoretical modeling of other seismic parameters (*19*). Because the waveguide disrupted at the fault bend and the rupture hesitated at the bend, which would tend to reduce P, we tentatively conclude that the waveguide is the result of dynamic rupture during the Landers event.

REFERENCES AND NOTES

1. C. H. Scholz, *The Mechanics of Earthquakes and Faulting* (Cambridge Univ. Press, New York, 1990); W. D. Mooney and A. Ginzburg, *Pure Appl. Geophys.* **124**, 141 (1986).
2. V. F. Cormier and P. Spudich, *Geophys. J. R. Astron. Soc.* **79**, 411 (1984); Y.-G. Li, P. Leary, K. Aki, P. Malin, *Science* **249**, 763 (1990); Y.-G. Li and P. C. Leary, *Bull. Seismol. Soc. Am.* **80**, 1245 (1990); A. Michelini and T. V. McEvilly, *ibid.* **81**, 524 (1991).
3. Y.-G. Li, K. Aki, D. Adams, A. Hasemi, W. H. K. Lee, *J. Geophys. Res.* **99**, 11705 (1994).
4. W. H. K. Lee, Y.-G. Li, R. Banfill, D. A. Dodge, *U.S. Geol. Surv. Open-File Rep.*, in press.
5. A joint field experiment between the Southern California Earthquake Center and the U.S. Geological Survey at Menlo Park.
6. P. C. Leary, Y.-G. Li, K. Aki, *Geophys. J. R. Astron. Soc.* **91**, 461 (1987); Y.-G. Li, P. C. Leary, K. Aki, *ibid.*, p. 485.
7. D. J. Wald and T. H. Heaton, *Bull. Seismol. Soc. Am.* **84**, 668 (1994).
8. B. P. Cohee and G. C. Beroza, *ibid.*, p. 692.
9. A. M. Johnson, R. W. Fleming, K. M. Cruikshank, *ibid.*, p. 499.
10. K. Sieh *et al.*, *Science* **260**, 171 (1993).
11. S. L. Beck and L. J. Ruff, *J. Geophys. Res.* **90**, 6773 (1985); T. M. Boyd and J. L. Nabelek, *Bull. Seismol. Soc. Am.* **78**, 1653 (1988); H. Houston and E. R. Engdahl, *Geophys. Res. Lett.* **16**, 1421 (1989); L. Dorbath *et al.*, *Geophys. J. Inter.* **108**, 309 (1992); M. Kikuchi, H. Kanamori, K. Satake, *J. Geophys. Res.* **98**, 15797 (1993); C. J. Ammon, T. Lay, A. A. Velasco, J. E. Vidale, *Bull. Seismol. Soc. Am.*, in press.
12. W. H. Bakun *et al.*, *Science* **225**, 288 (1984); G. C. Beroza and P. Spudich, *J. Geophys. Res.* **93**, 6275 (1988); A. J. Michael, *Bull. Seismol. Soc. Am.* **78**, 1199 (1988).
13. R. H. Sibson, *Philos. Trans. R. Soc. London* **317**, 63 (1986).
14. W. Thacher and M. G. Bonilla, in *Fault Segmentation and Controls of Rupture Initiation and Termination*, D. P. Schwartz and R. H. Sibsons, Eds. (U.S. Geological Survey, Palm Springs, CA, 1988), vol. 89-315, p. 386.
15. A. S. Papageorgiou and K. Aki, *Bull. Seismol. Soc. Am.* **73**, 953 (1983); K. Aki, *Tectonophysics* **211**, 1 (1992).
16. J. Boatwright, *Bull. Seismol. Soc. Am.* **72**, 1049 (1982); *ibid.* **78**, 489 (1988).
17. R. A. Harris and S. M. Day, *J. Geophys. Res.* **98**, 4461 (1993); E. Fukuyama and T. Mikumo, *ibid.*, p. 6529; H. Quin, *Tectonophysics* **175**, 93 (1990); K. Aki, in (*14*), pp. 1–9; C. H. Scholz, *Geology* **15**, 493 (1987).
18. C. H. Scholz, N. H. Dawers, J.-Z. Yu, M. H. Anders, P. A. Cowei, *J. Geophys. Res.* **98**, 21951 (1993).
19. Y. Ida, *Bull. Seismol. Soc. Am.* **63**, 959 (1973); K. Aki, *J. Geophys. Res.* **92**, 1349 (1987); C. Marone and B. Koyanagi, *Nature* **362**, 618 (1993).
20. E. Haukkson, L. M. Jones, K. Hutton, D. Eberhart-Phillips, *J. Geophys. Res.* **98**, 19835 (1993).
21. J. E. Vidale, *Bull. Seismol. Soc. Am.* **80**, 493 (1990).

22. We thank R. White, D. Harlow, S. Maichnick, and R. Banfill for helping to deploy the seismometers; G. Beroza, J. Boatwright, and W. Mooney for providing insight into fault zone structure; H. Houston and C. Sammis for improving the manuscript; E. Haukkson for providing unpublished relocations of Landers aftershocks; and K. M. Cruikshank and an anonymous reviewer for useful comments and suggestions. Supported by the Southern California Earthquake Center under National Science Foundation grant EAR-8920136 and U.S. Geological Survey grant 14-0A-0001-A0899.

5 April 1994; accepted 31 May 1994

Stepwise Formation of Multilayered Nanostructural Films from Macromolecular Precursors

Elaine R. Kleinfeld and Gregory S. Ferguson*

Sequential adsorption of a cationic polyelectrolyte and individual sheets of the silicate mineral hectorite has allowed controlled, stepwise formation of multilayered films on silicon wafers. Each component adsorbs rapidly by an ion-exchange mechanism, and x-ray diffractometry indicates structural order even in films with thicknesses greater than 0.2 micrometer. The large lateral extent of the silicate sheets (about 25 to 35 nanometers) allows each layer to cover any packing defects in the underlying layer, thus preserving structural order in the growing film. With careful choice of component materials, this method should allow for the preparation of multilayered films with a variety of technologically important properties.

Ultrathin films and multilayered structures are important for many applications, including x-ray optics (*1*), nonlinear optics (*2*), and microelectronics (*3*, *4*), and are under investigation for use as chemical sensors (*5*). Langmuir-Blodgett (LB) deposition (*6–8*) of preformed monolayers from a gas-liquid interface to a solid planar substrate can provide well-ordered, densely packed mono- and multilayered systems useful for these applications. Unfortunately, LB multilayers are mechanically unstable, held together primarily by van der Waals forces (*7*, *8*). Spontaneous self-assembly (SA) of molecular adsorbates onto solid substrates (*7*) can also provide densely packed monolayers and has recently been extended to the formation of multilayers in selected systems (*5*, *9*, *10*). The presence of covalent bonds or ionic attraction between layers provides additional stability not seen in LB systems; however, in many SA systems, adsorption of multilayers displaying structural order has proven difficult. In this report, we describe a method for the stepwise preparation of ordered multilayered films from ultrathin (~1 nm) layers of organic and inorganic macromolecules.

Department of Chemistry, Lehigh University, Bethlehem, PA 18015, USA.

*To whom correspondence should be addressed.